Article

New Synchronous Machine Rotor Design for Easy Insertion of Excitation Coils Based on Surrogate optimization

Tiejiang Yuan[1], Nan Yang[3], Wenping Cao[3], Zheng Tan[2], Guofeng Li[1], Xueguan Song[1]

1 Dalian University of Technology, Faculty of Electronic Information and Electrical Engineering, China

2 National Grid, China

3 School of Engineering and Applied Science, Aston University, Birmingham B4 7ET, United Kingdom

Correspondence: yangn1@aston.ac.uk

Abstract: This paper introduces a new rotor design for the easy insertion and removal of the rotor windings. The shape of the rotor is optimized based on surrogate method in order to achieve the lowest power loss under the maximum power output. The performance of the new rotor is examined in 2-D finite element software and validated by experiments. This rotor shows good potentials for reducing the maintenance and repair costs of synchronous machines, making it suitable for manufacturers within the mass production markets such as gen-sets, steam turbines, wind power generators and hybrid electric vehicles.

Keywords: Asymmetrical rotors, synchronous machine design, surrogate optimization.

1. Introduction

Synchronous machines are common machine type with numerous industrial applications especially in power generation. It is still considered as the universal machine for electric power generation including diesel/gas/steam turbines in heat power plants [1], large hydro-machines in hydro plants [2], and wind turbines in wind farms [3]. The wind turbine is typically assisted by gearboxes or power converters to operate in variable-speed mode in contrast to its normal constant-speed operation.

Even though Permanent magnet synchronous machines are becoming popular in recent decades due to their high-power density, wound rotor synchronous machines are still irreplaceable due to their high reliability in harsh operational environments. One major issue with the manufacture of wound rotor synchronous machines is its rotor winding process, which is considered to be quite laborious as the windings are not pre-designed and need to be wrapped around the rotor pole.

Two alternative methods have been proposed in industrial fields to simplify the manufacture process; however, they both have their drawbacks. A pre-manufactured rotor winding that is installed directly on the rotor tips separating it from the rotor pole. However, this would definitely affect the subsequent integration of the rotor. On the other hand, introduction of extra winding machines can simplify the winding process. The rotor will be placed on a winding machine and automatically wound with the rotation of the winding machine; but the economic cost of the winding machine would increase with the size of the rotor.

A new winding method is helpful for not only the new machines but also for rewound machines. When synchronous machines fail in the field and a rewinding is generally required [4], broken windings should be uninstalled in a way that is opposite to the installation [5]. A new rotor structure is proposed in a previous article [6], which modifies the geometry shape of the rotor to accommodate the excitation windings. The result shows that asymmetrical rotor design suffers from distributed waveform and low efficiency. Therefore, the optimization plan of the rotor is shown in this paper

Peer-reviewed version available at Energies 2018, 11, 1311; doi:10.3390/en11051311

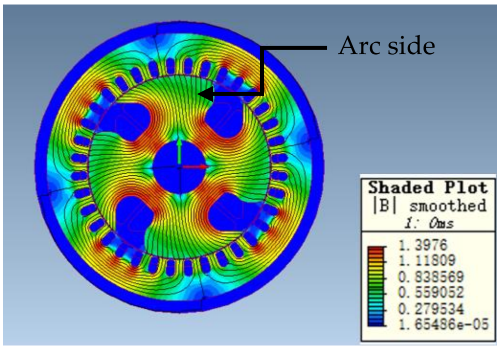

a

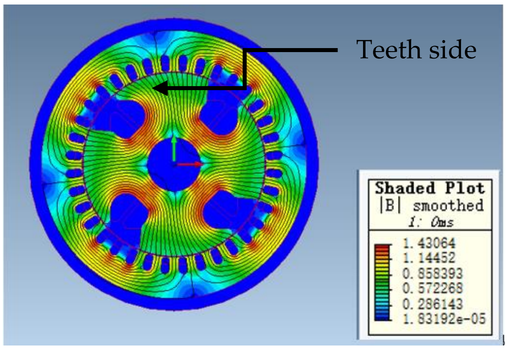

b

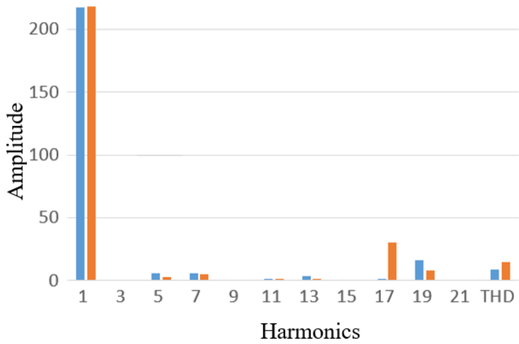

c

Fig. 1. *Changes in rotor geometry and their corresponding performance.*

(a)Enlarging the arc side, **(b)**Cutting the teeth side, **(c)** FFT analysis of induced emf

2. Original design analysis

The aim of this design is to change the shape of the rotor in a manner which allows the excitation coils to be easily installed directly on to the rotor pole. Therefore, part of the rotor tip is cut so that the excitation coil can be wound separately, and slid through the tip of the rotor onto the rotor pole, which is then fixed in position by a non-magnetic shield to offset the centrifugal force.

Two 4-pole machine numerical models are built in Magnet. The stator of both models come from a standard 27.5kVA alternator in the previous work [6]. The new rotor is used as an alternative to compare with the traditional design. As discussed in the previous work [6], the machine operation is similar to a traditional synchronous machine as well as its induced EMF and flux linkage. One unique feature of this machine is the unbalance flux distribution caused by the asymmetrical pole shape. Due to the absence of the rotor tip, the flux path of the machine will be shifted away from the geometrical center. This feature is further examined as an increase of the high order harmonics. Also, due to the flux shift, the flux tends to concentrate on the salient side of the rotor, thus an asymmetrical machine reaches saturation earlier than the symmetrical as the excitation MMF increase.

3. Rotor optimization

According to the FFT results of the initial asymmetrical rotor, there exists a distributed wave which needs to be corrected. Therefore, the influence of both stator and rotor are examined as following:

Preprints (www.preprints.org) | NOT PEER-REVIEWED | Posted: 11 April 2018 doi:10.20944/preprints201804.0153.v1

Peer-reviewed version available at Energies 2018, 11, 1311; doi:10.3390/en11051311

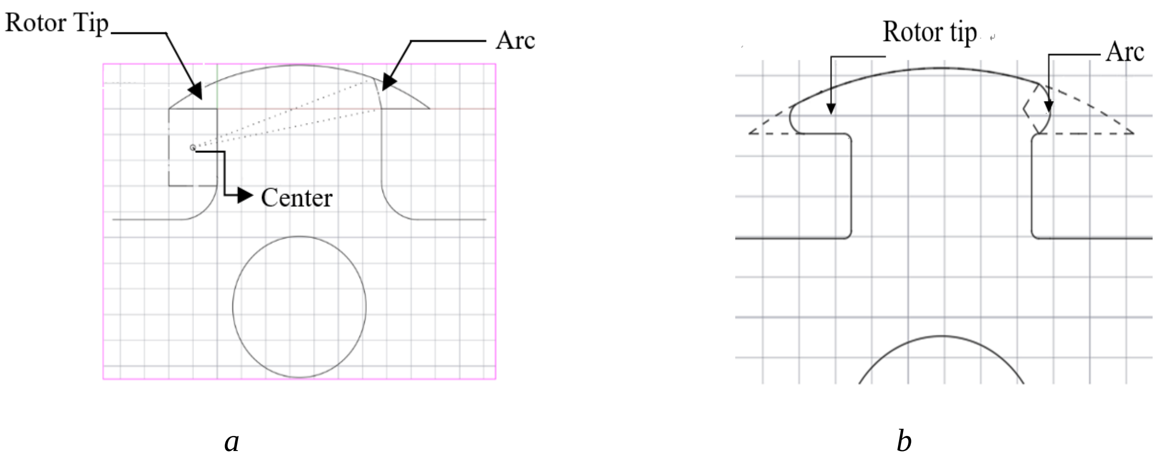

***Fig. 2** Optimization designs.*

3.1. Research on rotor shape

Asymmetrical rotor can be divided into two sides, the one with the teeth (teeth side) and the one without teeth (arc side). Adjustment on teeth side will change the flow of the flux, shifting the flux away from the center. On the other hand, changing arc side would guide the flux back to the center; however, it will also weaken the air-gap flux density. These changes both have influence on the harmonics as well as efficiency. Therefore, the shape of the rotor is a relative complex multi-input multi-output (MIMO) optimization problem. Flux distributions of both changes are shown in Fig. 1.

3.2. Optimizaion plans

The rotor shape of the original design is for easy insertion of excitation coil. However, as shown in the FEA as well as the experiment test, majority of the flux in the original rotor has been concentrated on the tips of the rotor due to the edge effect: magnetic field causes magnetic flux to follow along the path of least magnetic reluctance.

In this case, the tips of the rotor should be reshaped, avoiding rectangular edge (creating even flux path) whilst creating even air-gap distance around the edge of the rotor. Two design plans have been proposed and simulated as shown in Fig. 2.

Since the aim of this project is to develop a rotor structure for easy installation of the excitation winding, one side of the rotor tip has to be removed in order to slide the excitation windings onto the rotor pole. New rotor is optimized based on the rotor of one commercial synchronous machine.

Design 1 attempts to cut the right side of the rotor tip with an arc. This arc directly connects the rotor pole with the outside arc, which allows a smooth path for the flux to pass. It will separate the rotor into one side with rotor tip (refer as tip side) and one side without rotor tip (refer as arc side). The flux of the rotor can be modified by changing the direction of the arc. Therefore, the edge effect can be reduced.

4. Surrogate optimization method

Traditional rotor design includes both analytical and empirical methods. However, in this optimization, complexity of the rotor geometry makes it very difficult to be deduced analytically. On the other hand, empirical solution will be too simplified to reflect the effects of the change of rotor geometry.

Numerical methods, such as finite element method (FEM) take into account the complex topology of the electrical machine as well as its multi-physical characteristics [7]. It is proved to be able to predict the machine performance very accurately. However, it is also considered to be time-consuming and computationally expensive, due to the objective function needing to be evaluated for each set of structural parameters. Overall, a new optimization solution is required in this process.

The surrogate modelling technique is an effective tool for the analysis and optimization of computationally expensive models [8]. It provides a compromised solution between the high-fidelity low-speed calculations and high-speed low-accuracy simplified analytical methods.

Surrogate model is constructed by using the data obtained from high-fidelity models (in this design, FEM models), and it provides rapid approximations of objectives and constraints at new design points so that optimization studies are feasible [9].

The accuracy of surrogate models is evaluated by an error analysis. Once the surrogate model is proved to be accurate to predict the output, search algorithm could be applied on the surrogate model.

Since the aim of this project is to develop a rotor structure for easy installation of the excitation winding, one side of the rotor tip has to be removed in order to slide the excitation windings onto the rotor pole. New rotor is optimized based on the rotor of one commercial synchronous machine.

Design 1 attempts to cut the right side of the rotor tip with an arc. This arc directly connects the rotor pole with the outside arc, which allows a smooth path for the flux to pass. It will separate the rotor into one side with rotor tip (refer as tip side) and one side without rotor tip (refer as arc side). The flux of the rotor can be modified by changing the direction of the arc. Therefore, the edge effect can be reduced.

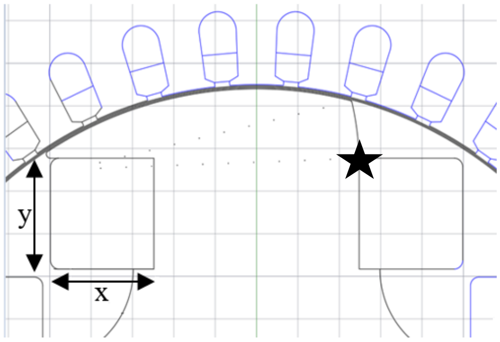

Fig. 3. *Problem definition A of Design 1.*

4.1. Problem definition

The first step of this optimization is to determine the shape with variables. Problem definition A of Design 1 is shown in Fig.3. The principle of the Design is simple, since the joint point between the rotor pole and rotor body (star marker in Fig.3.) is fixed, an arc can be easily defined by its arc center (x,y) which connects the point with star mark to the outside arc. In this case, the optimization is clearly a 2-variable optimization (x and y). The optimization plan is defined as:

Maximize: Power output

Minimize: Power Loss

$$\text{Constraints: } \begin{cases} 0 \le x \le 20 \\ 0 \le y \le 20 \end{cases} \tag{1}$$

This optimization is defined to locate the best performance of the machine which means maximum torque should be achieved with minimum loss.

4.2. Simplified analytical method

Based on the problem definition, the air-gap flux density of this rotor is obviously altered due to the variation of air-gap length. Therefore, the effect of this rotor shape is analytically computed in this section.

For estimating the average airgap distance: main geometries should be transferred into polar form as shown in Fig.4.

Stator and rotor: ρ=Rs; ρ=Rr

Arc:

$$\begin{aligned} &(\rho\cos(\theta)-x_0)^2+(\rho\sin(\theta)-y_0)^2=r_3^{\,2} \\ &\textit{when } \theta<\rho<\theta_2 \end{aligned} \tag{2}$$

Preprints (www.preprints.org) | NOT PEER-REVIEWED | Posted: 11 April 2018 doi:10.20944/preprints201804.0153.v1

Peer-reviewed version available at *Energies* **2018**, *11*, 1311; doi:10.3390/en11051311

Assume:

$$\begin{cases} g(\theta) = 2y_0 \sin(\theta) + 2x_0 \cos(\theta) \\ C_2 = -a^2 - b^2 + 2ax_0 + 2by_0 \end{cases} \tag{3}$$

The equation can be simplified into:

$$\rho = \frac{-g(\theta) \pm \sqrt{g(\theta)^2 - 4C_2}}{2} = f(\theta) \tag{4}$$

Air-gap distance could be calculated as

$$l(\theta) = \begin{cases} 2 & \theta_{rs} < \theta < \theta_1 \\ \sqrt{(f(\theta))^2 + R_s^2 - 2f(\theta)R_s} & \theta_1 < \theta < \theta_2 \end{cases} \tag{5}$$

The average air-gap distance over one rotor pole pitch (one out of four in a four-pole rotor) is calculated as:

$$L_{avg} = \frac{1}{\tau_{pole}}\left[\int_{\theta_{rs}}^{\theta_1} 2d\theta + \int_{\theta_1}^{\theta_2} l(\theta)d\theta\right] \tag{6}$$

when saturation and flux leakage are neglected, average flux density could be calculated as:

$$B_{avg} = \frac{B_r}{\frac{A_g}{A_m} + \mu_r \frac{L_{avg}}{l_m}} \tag{7}$$

The peak-to-peak open-circuit flux linkage is given by:

$$\Phi_p = B_{avg} \pi DL/2p \tag{8}$$

Back EMF and torque can be expressed as:

$$\begin{aligned} E_{avg} &= K_{dpn} \frac{2N\Phi_p}{\frac{2\pi}{2p\omega_r}} = 2K_{dpn} Np\Phi_p \omega_r \\ &= K_{dpn} N\pi B_{avg} DL\omega_r \end{aligned} \tag{9}$$

The torque is given by:

$$T = \frac{P}{\omega_r} = \frac{E_{avg} I}{\omega_r} = \frac{\pi}{2} K_{dpn} \pi D^2 L B_{avg} Q \tag{10}$$

where a, b, x0, y0 and the expand angle of the arc

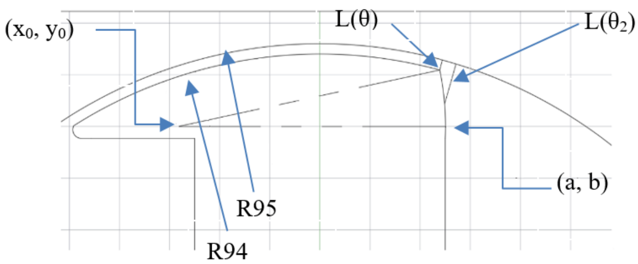

Fig. 4. *Analytical definition of Design 1.*

According to the calculation, the average torque depends on the average air-gap flux density, which is influenced by the corresponding constants. Since the coordinates a and b are fixed based on the prototype, the two variables influencing the torque performance are x0 and y0, i.e. the coordinates of the center.

However, this calculation is relatively low-accurate due to the high-level of saturation on rotor and irregular flux path in this design. Therefore, surrogate method is applied in this design.

Peer-reviewed version available at Energies 2018, 11, 1311; doi:10.3390/en11051311

4.3. Design of experiments

Design of experiment is aimed to collect the maximum information in the minimum sampling points in the design spaces [11, 12, 13]. It is designed to reduce the random error and bias error in the sampling process and to make the surrogate model more accurate.

Latin Hypercube sampling [15] is a typical type of modern DoE technology widely used in computation. Two aspects of LHS show its advantage over the other methods. Firstly, LHS can provide a more accurate estimation of the mean value. Secondly, it is not restricted by the size of the sampling points. Therefore, it would allow the user to control the complexity and computation cost of the sampling.

The design spaces of LHS are divided into several bins with the same probabilities. The generation of sampling points are based on two principles: 1. The generation of each sampling points is independent and randomly selected. 2. Only one point is allowed in each bin.

A simple mathematical equation for generating LHS sampling points is:

$$x_j^{(i)} = \frac{\pi_j^{(i)} + U_j^{(i)}}{k} \tag{11}$$

for $1 \leqslant j \leqslant n$ and $1 \leqslant i \leqslant k$

where k is the number of samples, n is the number of design variables, U is a uniform value on [1,0], π is an independent random permutation of the sequence of integer 0, 1…, k-1. Subscript j donates the dimension number and superscript i donates the sample number.

As an improvement, over unrestricted stratified sampling method, LHS can be applied to design variables that have abnormal probability distribution as well as correlations among the variables [16]. Therefore, it is adopted as the preferred DoE technique in this work.

4.4. Construction of surrogate models

Following an appropriate generation of sampling points, a suitable approximation approach is chosen in the next step. Kriging model has become the most popular surrogate model construction method in recent years. Math function of Kriging model is composed of two components: one polynomial model, and one isolated symmetrical component; representing either small scale, high frequency variation of large scale, or low frequency variation, with the basic assumption that these fluctuations are correlated only by the distance between the locations under consideration [17]-[18]. To be more specific, a zero-mean second-order stationary process is expressed by the following equations:

$$y(t)=\beta+z(t) \tag{12}$$

where β is a constant value, and fundamental function z(t) is Gaussian distribution with error. The residual error is considered to either independent, identically distributed or normal random variables with zero mean and variance. Similar to the previous model, the estimate model for y(t) can be expressed by:

$$\hat{y}(t) = \hat{\beta} + r^T R^{-1}(y - \hat{\beta} q) \tag{13}$$

where R is the correlation matrix, r is the correlation vector, y is the ns observed data vector, and q is unit vector. The correlation matrix and vector are:

$$R(t^j, t^k) = Exp[-\sum_{i=1}^{n} \theta_i \left| t_i^j - t_i^k \right|^2] \tag{14}$$

where i and j are independent indices from No.1 to No. ns (number of samples)

$$r(t) = [R(t, t^{(1)}), R(t, t^{(2)}), \ldots, R(t, t^{(ns)})]^T \tag{15}$$

The parameters θ1 to θn should be calculated as and solved by applying optimization algorithm:

Peer-reviewed version available at Energies 2018, 11, 1311; doi:10.3390/en11051311

$$\text{maximize} - \frac{[n_s \ln(\hat{\sigma}^2 + \ln|R|]}{2} \tag{16}$$

Significant number of studies have been conducted to compare the precision of the estimated models and Kriging method is considered to be more accurate in predicting non-linear and complex real models. Therefore, Kriging model is employed in the surrogate modelling of this paper.

4.5. Heuristic search method

After the construction model, search method should be applied in order to locate the local best performance. Compared to other computational intelligence-based techniques, Particle Swarm Optimization has its advantages in easy implementation, more effective memory capability, and more efficient in maintaining the diversity of the swarm [19]. Therefore, it is selected to be used in the optimization.

5. Optimization Results

Two optimization plans with different problem definitions are shown in this section.

5.1. Results and Analysis of Preliminary Surrogate Models

This surrogate optimization uses 50 training points. After training, the surrogate model is shown in Fig. 5. Surrogate model shows that the torque is distribute linearly. Higher torque is always achieved in top right corner of the design region. However, the loss is quite non-linear and distribute unequally around the whole design regions.

By using PSO search algorithm, the surrogate optimization gives their estimation. The optimal point is set at [15.55, 17.94], where the estimate torque is 173Nm and estimate loss is 374.99W.

To conclude, these simulation shows that by changing two variables, the performance will not be improved significantly. The torque improvement is less than 1%, and loss is reduced by less than 10W. Thus, more variables should be used in order to design a rotor shape which has significant influence on the machine performance.

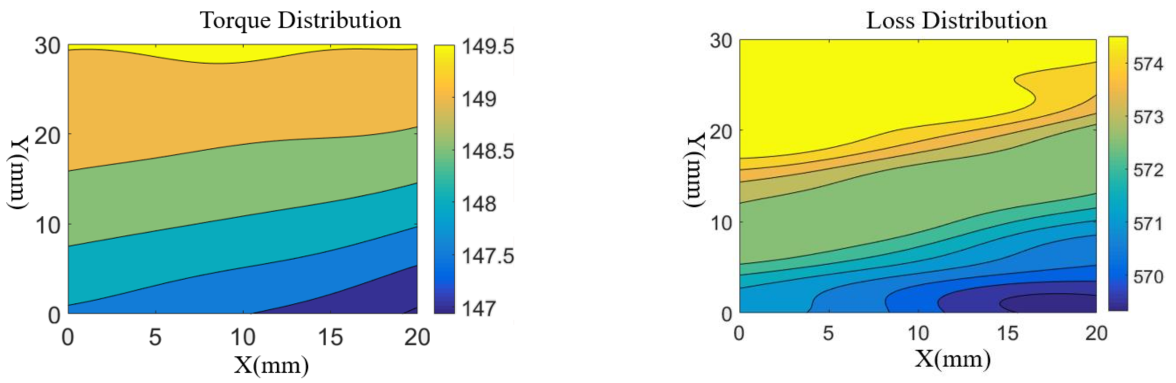

a *b*

Fig. 5. *Preliminary surrogate results*

(a)Torque contour, **(b)**Loss contour

5.2. Results and Analysis of Advanced Surrogate Models

Problem definition B of Design 1 is shown in Fig.6(a). The principle of the design is an extended version of problem definition A, which added two more variables into the design spaces.

These added variables are used to cut the tip-side of the rotor in order to balance the flux distribution. The aim of the optimization stays the same:

Maximize: Power output

Minimize: Loss

Constrains: $0<x<20$, $0<y<30$, $2<R<10$, $27<\theta<36$

Peer-reviewed version available at *Energies* **2018**, *11*, 1311; doi:10.3390/en11051311

Problem definition C of Design 2 is shown in Fig. 6(b). This version is a little more complex compared to problem definition B. In order to balance the flux distribution, the arc side of the rotor tip is not completely removed. In addition to that, the left side of the rotor is also cut with a circle. Two additional round circles are added to guide the flux into the rotor to avoid rectangular contact. As a result, this Design is a 4-variable optimization plan similar to Design B. The optimization goal is shown:

Maximize: Power output

Minimize: Loss

Constrains:0<R1<6, 0<R2<4, 0<L1<6, 0<R4<4

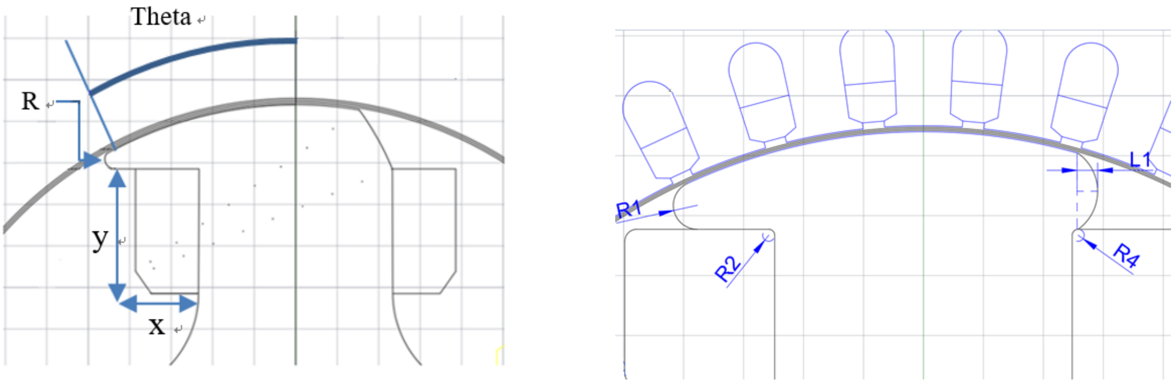

a *b*

Fig. 6. *Advanced problem definition*

(a)Design 1, **(b)**Design2

As shown in Fig.7, flux paths of both designs are shifted towards the tip side of the rotor due to the absence of rotor tip. However, it is clear that Design 2 provide a better flux distribution. The flux concentration on the rotor tip is reduced by providing extra flux path on the arc side. This has a clear influence on the induced EMF of the two designs.

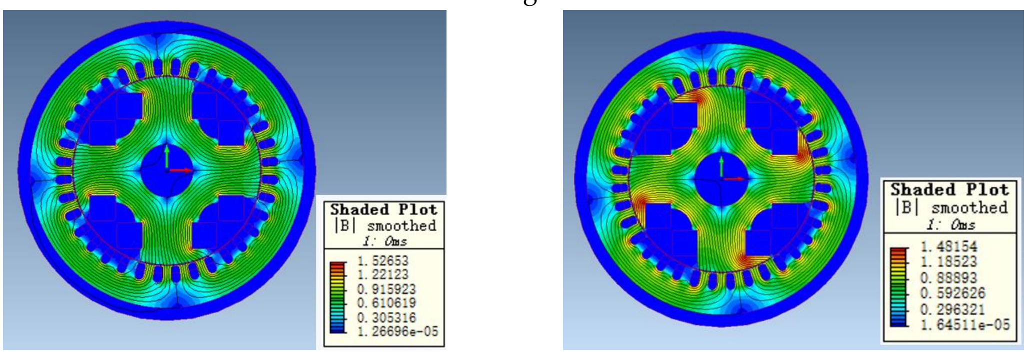

a *b*

Fig. 7. *Flux distribution of two optimized rotors*

(a)Design 1, **(b)**Design2

According to the FFT results in Tab. 1 and Fig.8(a), it is noticed that induced EMF is significantly distorted in design 1. This is a clear reflection of the unbalanced flux path. However, in the second Design, since the flux is distributed evenly on both sides, total harmonic distortion is remaining at an acceptable level.

Another interesting aspect of the two designs is the saturation level. As stated in the previous design, saturation level should be carefully examined due to the high flux concentration on the rotor tip. Fig. 8 shows a comparison of EMF among the two designs and the original rotor design.

No-load characteristic shows that both Design 1 and Design 2 are not easy to saturate. However, it also shows they would have a relative low voltage in the given excitation level. This can be expressed by the reduction of the flux paths due to the removal of the rotor tip. However, it is worthy of note that both designs achieve higher voltage at the expense of higher excitation level.

Preprints (www.preprints.org) | NOT PEER-REVIEWED | Posted: 11 April 2018 doi:10.20944/preprints201804.0153.v1

Peer-reviewed version available at *Energies* **2018**, *11*, 1311; doi:10.3390/en11051311

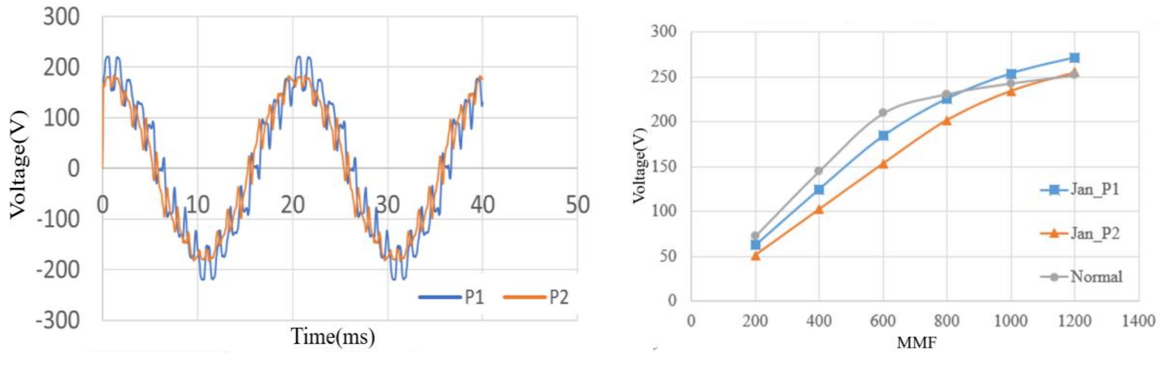

a *b*

Fig. 8. *Comparison of two optimized rotor*

(a)Comparison of the induced EMF, **(b)**Comparison of no-load saturation characteristic

In general, the two designs operate similar to normal symmetrical rotor. The maximum power generated by the two designs are higher than the traditional symmetrical rotor. An interesting factor is the maximum power angle. As shown in Fig. 9, the maximum power angle is quite different in the two designs. This is as a result of the unique shape of the rotor and its flux path.

As described above, both design plans show different characteristic and each should have its own merits and drawbacks. Therefore, it is very hard to decide which one should be applied. Optimization should be carried out in order to find the best performance of the two different designs.

Since the advanced optimization plans are 4-variable optimization, the results cannot be visualized as the previous 2-D figure. Following the same pattern, details of optimization results are shown in Table. 2.

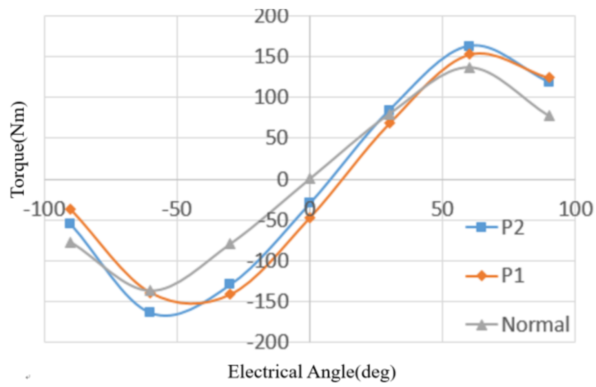

Fig. 9. *Comparison of torque-angle of the two designs.*

The accuracy of the surrogate model is confirmed by the FEA simulation. According to the results, both designs have similar iron losses. Both designs also perform better in reducing iron loss compared to the original asymmetrical design. However, compared to the original design, the torque provided by Design 1 has been decreased significantly. Therefore, it is not ideal for our optimization goal. As a result, Design 2 is selected for the experiment prototype validation. Detail simulation results with experimental validation are discussed in the next section.

TAB. 1. FFT results of the induced EMF

Harmonics	P1(V)	P2(V)
1	184.61	173.29
3	0.03	0.04
5	9.26	7.08
7	1.91	4.17
9	0.12	0.18
11	0.70	2.85

13	4.26	1.87
15	0.05	0.05
17	34.78	7.92
19	0.5	16.13
THD	0.2	0.12

TAB. 2. Optimized results of two rotors

Item	Design 1	Design 2	Preliminary Prototype
X1	21.65	4	/
X2	24.72	1.33	
X3	2	2	
X4	27	2	
Torque (FEA)	154.68 Nm	163.54 Nm	162.5 Nm
Torque (Surrogate)	154.73 Nm	163.70 Nm	
Loss (FEA)	424.3 W	462.5 W	544.4 W
Loss (Surrogate)	422.9 W	462.48 W	

6. Experiment validations

After a round of optimizing the rotor design and analyzing the machine performance, the rotor design is finalized and the rotors are prototyped, as shown in Fig. 10. Specifications of the prototype is given by Tab. 3.

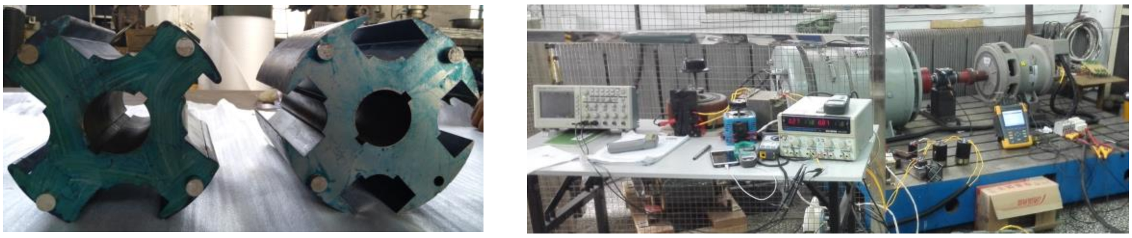

a *b*

***Fig. 10.** Photographs of the test rigs.*

(a)Symmetrical and asymmetrical rotor lamination, **(b)**Test rigs

Stator of the machine is a duplicate of a standard Cummins PI-144F machine. In order to reduce the major influence of the manufacture process, two rotors are made by the same manufacturer. For stator windings, they are 2/3 short-pitched double-layer star connected windings with 144 mm2 for each layer. For rotor windings, 76 turns of copper coil (2.3 mm radius each) are used on rotor coils.).

TAB. 3. Specifications of the prototype

Rated Power (kVA)	27.5	Rated Speed (rpm)	1500
Rated Line Voltage (V)	380	Rated Frequency (Hz)	50
Rated Power Factor	0.8	Stack Length (mm)	200
Stator Slot Number	36	Pole Numbers	4
Stator OD (mm)	310	Stator ID (mm)	192
Rotor OD (mm)	188	Winding arrangement	Double-layer Star

6.1. Constant speed-variable excitation test

A constant speed-variable excitation test is conducted by coupling the test machine with a DC drive motor. The machine is driven by the DC motor to the synchronous speed with open-circuit connection under rated excitation. Results of both rotors are shown in Fig. 11.

When compared with the symmetrical rotor, it is clear that the prediction of the FEA is lower than the experiment results by roughly 10%. Prediction of the asymmetrical rotor is quite close to the experiment in lower excitation level but gets into saturation faster than predicated. However, both no-load characteristic shows that asymmetrical rotor could perform similar to symmetrical rotor at the expense of higher excitation level.

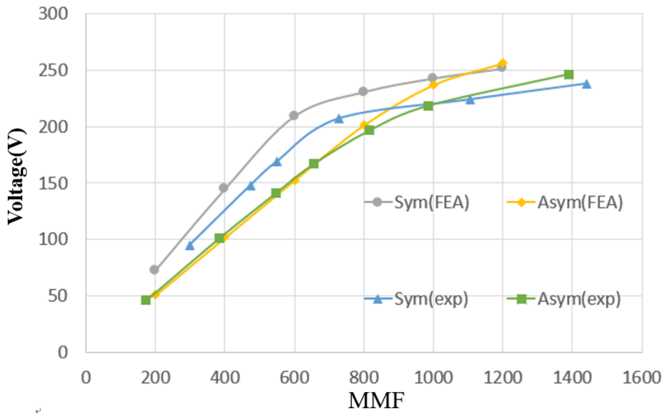

Fig. 11. *Comparison of the constant speed-variable excitation test.*

6.2. Analysis of experiment results

As stated in [19], for each of the values of voltage 50 % or less from constant speed-variable excitation test, a curve of constant losses against open circuit voltage U02 is developed and extrapolated on a straight line up to zero voltage. The intercept with the zero-voltage axis is the windage and friction losses Pfw. The iron loss of the machine can be obtained by taking off Pfw in the constant power loss PK under rated open circuit voltage. The power curve is shown in Fig.12 and calculation results are shown in Tab. 4.

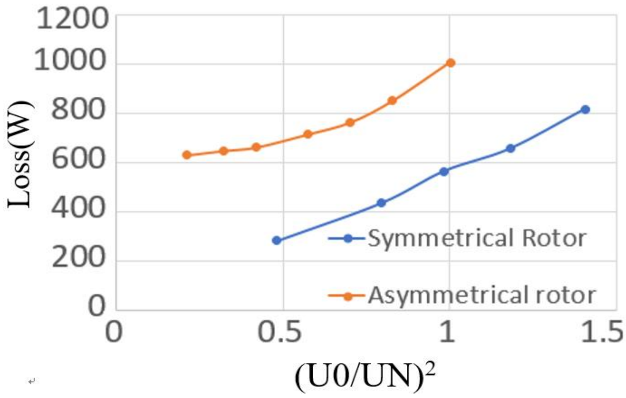

Fig. 12. *Power losses of the constant speed-variable excitation test.*

It is noticed that experimental results are slightly lower than FEA anticipation. This is partly due to the fact that material characteristic for the simulation is inaccurate compared to the actual material used in experiment. However, it still confirmed that the loss of asymmetrical rotor can reach the same level as in symmetrical rotor and it is significantly better than the initial design.

Attention should be paid to the friction and windage losses of the asymmetrical rotor, which is larger than the symmetrical rotor. Unbalance shape of the asymmetrical rotor makes a larger vibration, increasing the mechanical loss of the machine, similar to the studies on asymmetrical PMSM in [22]. Therefore, the alignment of the shaft and the fixing of the frame should be specially designed.

Preprints (www.preprints.org) | NOT PEER-REVIEWED | Posted: 11 April 2018 doi:10.20944/preprints201804.0153.v1

Peer-reviewed version available at *Energies* **2018**, *11*, 1311; doi:10.3390/en11051311

TAB. 4. Specifications of the prototype

	Symmetrical rotor	Asymmetrical rotor	Preliminary asymmetrical design
FE analysis	470 W	463 W	544 W
Experiment	408 W	407 W	493 W

6.3. Low-slip test

This saliency caused by rotor shape has its impact on the torque output of the alternator. Per the equations in [20], the output torque at any speed can be derived as:

$$T = X_{ad} I_f I_s \cos\gamma - \frac{1}{2}(X_d - X_q) I^2_s \sin 2\gamma \qquad (16)$$

where Xd and Xad are the per unit direct axis synchronous and magnetizing reactance at one per unit speed, Xq is the per unit quadrature axis reactance at one per unit speed; and Is is defined as the phase current.

In (16), the first component of the equation represents the torque generated by the round rotor and the second part is the reluctance torque caused by the saliency of the rotor. Reluctance torque is influenced by the asymmetrical rotor structure in the optimization and total power is increased.

The measurement of the direct-axis reactance and quadrant-axis reactance is carried by a low-slip test following the standard method [19]. Comparison of the FEA simulation and experiment results are presented in Tab. 5.

TAB. 5. Slow-slip results of two designs

Item	Symmetrical	Asymmetrical
X_d(FEA)	19.24	16.34
X_d(Experiment)	18.75	15.4
X_q(FEA)	10.99	4.71
X_q(Experiment)	10.57	5.85

7. Conclusion

This paper has presented a new asymmetrical rotor topology which shifts the magnetic path to increase the cross-sectional area of saliency. The machine assembly and repair process is significantly simplified by this modification. The new rotor optimization focused on presenting the critical curvature of the rotor geometry by varying parameters, investigating the influence of the rotor shaping methods by surrogate models and optimizing the rotor pole shape for high-efficiency output.

Through the geometry boundary design, the machine is optimized to achieve a high-efficiency power output and still keep the easy installation feature. The influence of rotor shaping is proved by FEA simulations and experiment. Investigations indicate that the new rotor shape can achieve the same performance as the traditional rotor after optimization, with the added ease of rotor installation.

References

1. A. Setiyoso, A. Purwadi, B. Halimi and A. Rizqiawan, "Design of synchronous machine 10625kVA for small power-plant in Indonesia," *3rd Conference on Power Engineering and Renewable Energy (ICPERE)*, Yogyakarta, pp, 81-86, 2016.
2. A. Dietz, A. Groeger and C. Klingler, "Efficiency improvement of small hydroelectric power stations with a permanent-magnet synchronous machine," *1st International Electric Drives Production Conference, Nuremberg*, pp. 93-100, 2011.
3. S. Grabic, N. Celanovic and V. A. Katic, "Permanent Magnet Synchronous Machine Cascade for Wind Turbine Application," *IEEE Transactions on Power Electronics*, vol. 23, no. 3, pp. 1136-1142, May 2008.

4. G. Stone, I. Culbert, E. Boulter and H. Dhirani, "Salient pole rotor winding failure mechanisms and repair," *Electrical Insulation for Rotating Machines: Design, Evaluation, Aging, Testing, and Repair* ,Wiley-IEEE Press, Hoboken, NJ, USA, pp. 253–263, 2014.
5. N. Yang, W. Cao, Z. Liu, Z. Tan, Y. Zhang, S. Yu, J. Morrow, "Novel asymmetrical rotor design for easy assembly and repair of rotor windings in synchronous generators," *IEEE Magnetics Conference (INTERMAG)*, Beijing, pp. 1-1, 2015.
6. N.Yang, W. Cao, Z. Tan, X. Song, T. Littler and J. Morrow, "Asymmetrical rotor design for a synchronous machine based on surrogate optimisation algorithm," *8th IET International Conference on Power Electronics, Machines and Drives* , Glasgow, pp. 1-6, 2016.
7. T. W. Preston and J. P. Sturgess, "Implementation of the finite-element method into machine design procedures," *Sixth International Conference on Electrical Machines and Drives (Conf. Publ. No. 376)*, pp. 312–317, 1993.
8. Y. Duan and D. M. Ionel, "A Review of Recent Developments in Electrical Machine Design Optimisation Methods With a Permanent-Magnet Synchronous Motor Benchmark Study," *IEEE Transactions on Industry Applications*, vol. 49, no. 3, pp. 1268–1275, May 2013.
9. N. V. Queipo, R. T. Haftka, W. Shyy, T. Goel, R. Vaidyanathan, and P. Kevin Tucker, "Surrogate-based analysis and optimisation," *Progress in Aerospace Sciences,* vol. 41, pp. 1-28, 2005.
10. Z. Tan, X. Song, W. Cao, Z. Liu, and Y. Tong, "DFIG machine design for maximizing power output based on surrogate optimisation algorithm," *IEEE Trans. Energy Conversion*, Vol. 30, No. 3, pp. 1154-1162, Sep. 2015.
11. A. A. Giunta, S. F. Wojtkiewicz, M. S. Eldred, "Overview of modern design of experiments methods for computational simulations," *American Institute of Aeronautics and Astronautics*, 2003.
12. Santner, T.J. Williams, B. Notz, I. William, "The Design and Analysis of Computer Experiments," *Springer*, Heidelberg , 2003.
13. J. R. Koehler, A. B. Owen, "Computer experiments," *Handbook of Statistics*, vol. 13, pp. 261–308, 1996.
14. Z. H. Han and K. S. Zhang, "Surrogate-Based Optimisation," Technical report, School of Aeronautics, Northwestern Polytechnical University, Xian, P.R. China, 2012.
15. M. D. McKay , R. J. Beckman, and W. J. Conover, "A Comparison of Three Methods for Selecting Values of Input Variables in the Analysis of Output from a Computer Code," *Technometrics*, Vol. 21, No. 2, pp. 239-245, 1979.
16. M. Stein, "Large sample properties of simulations using Latin hypercube sampling," *Technometrics,* vol. 29, pp. 143-151, 1987.
17. M. J. Sasena, "Flexibility and efficiency enhancements for constrained global design optimisation with kriging approximations," *General Motors*, 2002.
18. N. V. Queipo, R. T. Haftka, W. Shyy, T. Goel, R. Vaidyanathan, and P. Kevin Tucker, "Surrogate-based analysis and optimisation," *Progress in Aerospace Sciences,* vol. 41, pp. 1-28, 2005.
19. A. P. Engelbrecht, "Particle swarm optimisation: where does it belong?," in *Proc. IEEE Swarm Intell. Symp.*, pp. 48-54, May 2006.
20. Rotating electrical machines - Part 4: Methods for determining synchronous machine quantities from tests, *BSI British Standards BS EN 60034-4*: 2008.
21. Liu W, Lipo TA.: "On saliency enhancement of salient pole wound field synchronous machines," *Energy Conversion Congress and Exposition (ECCE)*, IEEE; 2016.
22. A. J. Piña Ortega and L. Xu, "Investigation of Effects of Asymmetries on the Performance of Permanent Magnet Synchronous Machines," *IEEE Transactions on Energy Conversion*, vol. 32, no. 3, pp. 1002-1011, Sept. 2017.